Contribution of Thermal Infrared Remote Sensing Data in Multiobjective Calibration of a Dual-Source SVAT Model

Benoît Coudert, Catherine Ottle, B. Boudevillain, J. Demarty, P. Guillevic

Contribution of Thermal Infrared Remote Sensing Data in Multiobjective Calibration of a Dual-Source SVAT Model

BENOIT COUDERT, CATHERINE OTTLÉ, AND BRICE BOUDEVILLAIN

Centre d'étude des Environnements Terrestre et Planétaires, IPSL/UVSQ, Vélizy, France

JÉRÔME DEMARTY

INRA Avignon, Unité CSE, Domaine Saint Paul, Site Agroparc, Avignon, France

PIERRE GUILLEVIC

Division Eau, Laboratoire Central des Ponts et Chaussées, Bouguenais, France

(Manuscript received 14 March 2005, in final form 26 September 2005)

ABSTRACT

This study fits within the overall research on the usage of space remote sensing data to constrain land surface models (LSMs) (also called SVAT models for soil–vegetation–atmosphere transfer). The goal of this paper is to analyze the potential of using thermal infrared (TIR) remote sensing data for LSM calibration. LSMs are characterized by a large number of parameters and initial conditions that have to be specified. This model calibration is generally performed at a local scale by minimization between measurements and time series difference. Recent studies have shed light on the use of multiobjective approaches for performing calibration and for analyzing the model's sensitivity to input parameters. Such an approach has been implemented in the SEtHyS LSM (for "Suivi de l'Etat Hydrique des Sols," the French acronym for soil moisture monitoring) with the objective of assessing the information contributed by having knowledge of the remote sensing surface brightness temperature. For this purpose, the model calibration was performed in three different cases at field scale corresponding to different calibration design. The analysis of these numerical experiments permits the authors to show the contribution and the limits of TIR remote sensing data for LSM calibration, in various environmental conditions. The perspectives underline the potential of using a dynamic calibration methodology, taking advantage of the time-varying model parameters' influence.

1. Introduction

This paper discusses the possibilities of using TIR brightness temperatures to estimate the parameters of land surface models (LSMs). LSMs have been developed to represent the energy and mass transfers at the soil–vegetation–atmosphere interface. These models are widely used for meteorological, agronomical, or hydrological purposes at various temporal and spatial scales. Such models simulate the time series of surface variables like surface temperature, soil moisture, and surface energy fluxes, when provided with atmospheric forcing and information about vegetation growth and surface hydrologic and thermal initial conditions. Since the scales of the physical processes are generally smaller than the space–time truncations of the models, the process representation is necessarily conceptual, and the water and energy transfers are described with simplified parameterizations. These parameterizations have generally been developed empirically and involve many parameters that can sometimes be measured locally. At a larger scale (like a heterogeneous general circulation model grid), most of these parameters are conceptual and can be estimated from the soil and vegetation characteristics with a large uncertainty. Therefore, there is a need to develop methodologies to estimate these parameters at a scale representing the physical processes in order to obtain the best prediction of the surface variables. It can be noted that the modeling

Corresponding author address: Benoit Coudert, Centre d'étude des Environnements Terrestre et Planétaires, IPSL/UVSQ, 10-12, Avenue de l'Europe, 78140 Vélizy, France.
E-mail: benoit.coudert@cetp.ipsl.fr

is approximately the same when applied at the local scale (field scale) or the grid scale of general circulation models (GCMs).

Remote sensing data can be useful for the model's calibration task because it provides information at a scale representative of the surface processes. This information can be used in soil–vegetation–atmosphere transfer (SVAT) models if the remote sensing signals are related to the surface parameters or variables. These relations are ensured by the radiative transfer models that simulate the remote sensing signals at the level of the space instruments: for example, brightness temperatures in the thermal infrared (TIR) or in the microwave domains or solar reflectances. Therefore, in order to constrain LSM with satellite data, it is important to develop numeric tools coupling SVAT models and multispectral radiative transfer models.

From all the space measurements available, TIR data have proved to provide valuable information for surface energy budget monitoring (Diak et al. 2004). In fact, with a given viewing direction, TIR domain radiometers are able to measure the surface emitted longwave and the atmospheric radiations, both transmitted along the atmospheric path. A simple first-order modeling of the radiative transfer through the atmosphere and at the soil–canopy interface allows for the simulation of the directional spectral brightness temperature, which can be compared to radiometric measurements. It is important to note that the directional brightness temperature is the sum of all emitting object contributions within the instrument footprint. In the case of a vegetation cover, the emitted radiation is a complex composition of the contributions of the different elements of the surface, in a specific instrument viewing direction. Previous works have shown that this temperature may be approximated using a two-source (soil and vegetation) SVAT model and a simple radiative transfer representation (see, e.g., François 2002). The measurement of this temperature can therefore be related to soil and vegetation temperatures. With the directional effects resulting from different weights of the soil and the vegetation components, some authors have shown that bidirectional measurements are sufficient for retrieving both soil and vegetation temperatures (François et al. 1997; Menenti et al. 2001; Jia et al. 2003) or for estimating soil and vegetation fluxes (Norman et al. 1995).

In this study, our purpose is to evaluate the potential of TIR data for calibrating dual-source SVAT models. Since the soil and vegetation temperatures are determined by the energy and water transfers in the soil–vegetation–atmosphere continuum, the knowledge of these variables (or strongly linked ones like the directional brightness temperature) should be of interest for calibrating or constraining the associated physical processes. One of the difficulties is the dimensionality of the calibration problem. LSMs are characterized by a large number of parameters: for example, a simple SVAT model like the Interaction Soil Biosphere Atmosphere (ISBA) model (Noilhan and Planton 1989) contains 14 parameters, and a more complex scheme like version two of the Simple Biosphere Model (SiB2: Sellers et al. 1996) has 48 parameters to estimate. These parameters or initial states do not all have the same sensitivity and, thus, do not need to be estimated with the same accuracy. It is therefore important to identify the most influential parameters in order to reduce the dimensionality of the optimization problem and improve the calibration technique. Among numerous sensitivity analysis methods, multicriteria methods are well adapted to SVAT models because these models present many output variables, which are related to the different processes represented and to the different model parameters. Such an analysis allows for better understanding of the model functioning and the dominant processes during the studied time period. The multiobjective generalized sensitivity analysis (MOGSA: Bastidas et al. 1999) has been applied successfully in performing the sensitivity analysis of SVAT models. Moreover, the method may be extended to perform the calibration of the model, as suggested by Demarty et al. (2005). As a result, these authors proposed the multiobjective calibration iterative process (MCIP), which was used in this paper for analyzing the impact of the TIR brightness temperature on the model calibration. The purpose is to determine (i) how remote sensing TIR T_B is useful in model calibration and (ii) what physical processes can be constrained by the measurement of this variable during the whole crop growing and senescent period. Our dual-source SVAT model, SEtHyS (for "Suivi de l'Etat Hydrique des Sols," French acronym for soil moisture monitoring), was chosen and applied at field scale in the framework of the Alpilles-ReSeDA (Remote Sensing Data Assimilation) experiment (Olioso et al. 2002a; http://www.avignon.inra.fr/reseda/base/), for which all variables to implement, run, and calibrate the model as well as TIR data were available. The methodology is based on numerical calibration experiments for four time periods corresponding to different surface, climate, and vegetation conditions. It is applied to three scenarios corresponding to different uses of input calibration data:

- Scenario 1: Surface fluxes, reflected solar radiation, soil water contents, and TIR brightness temperatures are used for the calibration.

- Scenario 2: Same as scenario 1 but without TIR brightness temperature.
- Scenario 3: TIR data only are used for calibration.

After a brief description of the SetHyS model and the database (section 2), the methodology and the framework of the numerical experiments are presented (section 3). Section 4 focuses on the results of scenario 1. The calibration results of both scenarios 1 and 2 are discussed in section 5. Finally, section 6 presents the conclusions and the perspectives on the use of TIR data to calibrate SVAT models and proposes a methodology to take advantage of all information contained in the brightness temperature measurement.

2. The SEtHyS model and the Alpilles ReSeDA database

a. The model

The SEtHyS model (presented in appendix A) is a SVAT coupled with a radiative transfer model in the visible and infrared domains, where vegetation is considered as a semitransparent and turbid medium (Beer–Lambert approach), taking into account a multiple reflection between the soil and the canopy. This one-dimensional modeling of water and energy surface fluxes simulates the thermal infrared surface temperature and the soil water content at field scale.

Two sources, the soil and the overlaying vegetation, are separately considered to solve the mass and energy budgets. Soil is divided into two layers: a thin surface layer and the total root zone.

The formalism of the model is the same as in Deardorff (1978) for the computation of the fluxes and the state variables: ground and canopy temperatures, specific humidity and air temperature inside the canopy, and soil water contents. The representation of photosynthesis with the calculation of the stomatal conductance is the same as the SiB model described in detail in Sellers et al. (1992, 1996).

The upper boundary conditions consist of atmospheric forcing: incoming radiation, precipitation, air temperature, specific humidity, and wind speed above the surface at the reference level $Z_a = 2$ m. Leaf area index (LAI), vegetation height, and field irrigation are also input data of the model. A prescription of the 22 input parameters (for vegetation, soil, and initialization) is required to run the model (a list is shown in Table 2).

b. Dataset

Data used to perform the different numerical experiments come from the Alpilles-ReSeDA program. This field experimentation was initiated to improve evaluation of soil and vegetation processes from remote sensing data.

Numerous data were acquired over the Alpilles (southeast of France) flat crop fields area from October 1996 to November 1997. Data acquisition on specific fields dedicated to SVAT model "calibration" was more complete. In particular, we investigate in this study measurements from field 101, a winter wheat crop for which all the data to calibrate and run the SEtHyS model over the whole growing and senescent period between days of experiment (DOE) 387 (21 January 1997) and 525 (8 June 1997) are available. The measurements performed on field 101 consisted of

- atmospheric forcing measurements performed by the central meteorological station at the center of the experimental site with a 15-s time step and an averaging period of 20 min (like the model time step). Air temperature, vapor pressure, and wind speed were measured at 2 m above the ground; rainfall and field irrigation were also measured and included in the forcing dataset as model input variables.
- latent and sensible heat fluxes obtained by means of the Bowen ratio (BR) method (over the whole simulation period) and the eddy correlation (EC) method (period 440–460). However, the BR-deduced heat fluxes presented some cases of overestimations (bias of $+15$ W m^{-2}) and large scattering (rmse between 50 and 70 W m^{-2}) compared to EC-deduced heat fluxes. These fluxes have been reprocessed (Olioso et al. 2002a).
- net radiation measurements, incident solar radiation, and reflected solar radiation performed at a 3-m height above the canopy. These data were intercalibrated between the different instruments used.
- thermal infrared surface temperature T_B obtained by measurement of upward canopy radiation in the 8–14-μm waveband with an 18.5° zenith angle and a 16° field of view. Bare soil and canopy emissivities in the 8–14-μm spectra were also measured.
- plant property measurements like green LAI or canopy height interpolated to daily values.
- soil measurements including soil moisture, soil water potential profiles, soil temperature, hydrodynamic and thermal properties, and soil hydraulic conductivity. Soil moisture profile was measured with neutron and capacitive probes. To dispose of measurements during all simulation periods, we have used neutron probe data between DOE 387 and 475 (rainfall episode) and capacitive probe data from DOE 476 to the end of the crop cycle (DOE 542). Textural data pedotransfer functions allowed determining the soil pa-

TABLE 1. Characteristics of the four simulation periods.

Period	DOE	LAI	Vegetation height (cm)
P1	387–407	0.21–0.56	12–16
P2	440–460	1.45–1.90	32–43
P3	505–525	1.52–1.60	69–72
P	387–542	0.21–1.9	12–74

rameters using a retention curve and hydraulic conductivity derived from Van Genuchten modeling (free parameters in the following study). Last, deep soil temperature was measured at different depths every 15 s and averaged over a period of 20 min.

Four different simulation periods (see Table 1) were investigated in order to check accuracy, efficiency, and behavior (parameter sensitivity) of the SEtHyS model under various atmospheric forcing and vegetation phenological conditions. Period P1 spreads over 20 days between 21 January and 31 January; it is the period with the lowest LAI values (bare soil with sparse canopy). Period P2 between 15 March and 4 April corresponds to the wheat growing period with a regular soil drying (no precipitation). Period P3 between 19 May and 8 June is a well-developed canopy period and a senescent phase of wheat with very dry soil and two rainfall events (which occurred on DOE 519 and 523). Last, the period P includes the three previous periods and spreads over 155 days between 21 January and 25 June.

3. Presentation of the multicriteria analysis methodology

The SEtHyS model requires the specification of 22 parameters and initialization variables, listed in Table 2. In this section, the methodology used to perform model calibration is presented.

a. Global and multicriteria approach

The specification of the model's parameters has a direct influence on the system response. Thus, the first step when one wants to run a LSM is its calibration. This calibration consists in the optimization (hereafter

TABLE 2. List of parameters and initial variables with their initial uncertainty ranges.

	Name	Description (units)	Initial uncertainty range, all periods
		Optical properties	
1	ε_g	Bare soil emissivity	0.94–0.99
2	α_{sec}	Dry soil albedo	0.225–0.35
3	α_{hum}	Wet soil albedo	0.1–0.22
4	w_{inf}	Moisture parameter for albedo calculation	0.15–0.29
5	w_{sup}	Moisture parameter for albedo calculation	0.291–0.5
6	α_{sv}	Vegetation albedo	0.16–0.32
		Vegetation characteristics	
7	V_{max0}	Leaf photosynthetic capacity (Rubisco) (μmol m^{-2} s^{-1})	30–200
8	l_{gf}	Dimension of the leaf along the wind direction (m)	0.01–0.08
9	k_{wstr}	Empirical parameter for water stress calculation	0.01–0.1
		Ground properties	
10	p_{hc}	"Half critic" hydrologic potential (m)	−200–100
11	w_{max}	Saturated soil water content (m^3 m^{-3})	0.3–0.5
12	w_{resid}	Residual soil water content (m^3 m^{-3})	0.05–0.15
13	h_{VG}	Scale factor in the Van Genuchten retention curve model (m)	−1.161–0.251
14	n_{VG}	Shape parameter in the Van Genuchten retention curve model	1.168–1.331
15	K_{sat}	Saturated hydraulic conductivity (m s^{-1})	2.4×10^{-8}–2.7×10^{-6}
16	$a_{E\text{lim}}$	Empirical parameter for limit evaporation	1–50
17	$b_{E\text{lim}}$	Empirical parameter for limit evaporation	1–50
18	$\mathcal{T}_{\text{therm}}$	Correction coefficient of the volumetric soil heat capacity (J m^{-3} K^{-1})	0.5–2
19	dp_2	Root zone depth (mm)	200–2000
		Initial variables	
20	w_{g_0}	Initial soil surface water content (m^3 m^{-3})	period 1/period 2/period 3 0.32–0.49/0.18–0.27/0.15–0.22
21	w_{2_0}	Initial root zone water content (m^3 m^{-3})	0.30–0.46/0.26–0.39/0.20–0.30
22	bias_{T_2}	Error in deep soil temperature (K)	$-2 < \text{bias}_{T_2} < +2$

minimization) of a cost function dealing with the model-simulated output and observation data divergence.

Several optimization techniques have been documented in the literature. Young (1978), Spear and Hornberger (1980), and Hornberger and Spear (1981) suggest keeping a set of parameter combinations as a solution of the optimization problem. Actually, searching for a unique global optimum is not satisfactory because of the parameter interactions, nonlinearities in the modeling, and observation uncertainties used in the calibration process. They propose to distinguish "acceptable" and "nonacceptable" combinations of the model parameters, with "acceptable" sets ensuring the higher model realism compared to the data observation reference. The general methodology is well known as the regionalized sensitivity analysis (RSA) or HSY algorithm according to the first letter of the author's names. Yapo et al. (1998) extended the single-objective global optimization shuffled complex evolution algorithm from Duan et al. (1993), to a multiobjective version, filling in the gap by exploiting all useful information contained in the dataset. This methodology, called the MOCOM-UA algorithm (Yapo et al. 1998), was developed and applied in a hydrological model calibration context using two objective criteria (root-mean-square error and heteroscedastic maximum likelihood estimator). For the models that simulate different processes and output variables, it is important to perform both calibration and validation on multiple variables.

Therefore, Gupta et al. (1999) and Bastidas et al. (1999) developed a stochastic multiobjective approach using only one objective function (the rmse), but simultaneously taking into account several different surface variables. They applied a methodology called the multiobjective generalized sensitivity analysis (MOGSA) for studying multiobjective sensitivity analysis and calibration (with MOCOM algorithm) of a SVAT model, the biosphere–atmosphere transfer scheme (BATS: Dickinson et al. 1993).

This methodology has been applied by Demarty et al. (2004, 2005) on the Simple Soil Plant Atmosphere Transfer and Remote Sensing (SiSPAT-RS) model (Braud et al. 1995; Demarty et al. 2004) to analyze the model sensitivity and to propose a calibration methodology (MCIP: Demarty et al. 2005) for the parameters and the initial states.

b. Presentation of the MCIP methodology

1) *Definition of initial ranges* for each parameter: This task can be done from an a priori knowledge of the surface properties or from local measurements and an estimation of their temporal and spatial variability.
2) *Uniform random sampling* of the feasible parameter space: each parameter is drawn in the defined ranges (statistical Monte Carlo approach). An exception is for the hydraulic conductivity, for which the logarithm of the range values is sampled (very little values and large range). The saturated water content of the soil depends on the initial soil water contents to preserve the physical realism of the parameterization.
3) *Achievement of a set of simulations:* each parameter combination gives rise to a simulation (stochastic technique).
4) *Calculation of the cost function*: root-mean-square error between simulations and observations:

$$\mathrm{rmse}(X) = \sqrt{\sum_{i=1}^{n}\left(\frac{(\hat{X}_i - \tilde{X}_i)^2}{n}\right)}, \qquad (1)$$

where $\hat{X}_i$ and $\tilde{X}_i$ are, respectively, the simulated and observed variable at time i. The rmse is calculated on the n observations available for each monitored output variable considered.
5) *Pareto ranking* or simple sorting and partitioning of the simulations in acceptable or nonacceptable solutions: Construction of two ensembles of solutions is required.
6) *Detection of parameter sensitivity* by comparison of the maximal distance between the cumulative distribution of each parameter on both ensembles: The statistical Kolmogorov–Smirnorff test relates this maximal distance to a probability value. The application of thresholds to this probability value permits one to quantify the degree of parameter sensitivity.
7) *Reduction of variation ranges* for the sensitive parameters: the ranges of other parameters are kept unchanged.

This methodology is a pure stochastic approach (easy to implement) whereas the MOCOM-UA algorithm combines the strengths of deterministic and stochastic techniques.

The iteration of the procedure described above, where reduced ranges at step 7 become the "new" ranges at step 1, achieves the model calibration. Sensitive parameter ranges are reduced iteration by iteration and the process stops when the decreases of the criteria ranges are all lower than 10%. A maximal number of 10 iterations was fixed to limit the computing time.

In our application, the criteria are the rmse of seven simulated variables: the directional surface brightness temperature T_B (K) over 8–14-μm spectra, the surface and root zone soil moistures w_g, w_2 ($m^3\ m^{-3}$), the total latent heat flux over canopy LE ($W\ m^{-2}$), the ground

surface heat flux G (W m^{-2}), the sensible heat flux H (W m^{-2}), and the solar-reflected radiation aR_g (W m^{-2}). All of these variables have been measured during the Alpilles-ReSeDA field experiment.

4. Multiobjective model calibration

This section presents the application of the MCIP approach on the SetHyS model. The calibration dataset includes the measurements of seven simulated variables: T_B, w_g, w_2, G, H, LE, and aR_g. Note that the latent heat flux (LE) is not used for calibration but to control the consistency of the results for this variable. Moreover, measurements of LE do not contain more information than H flux to constrain the energy balance. In the methodology described above, the rmse of surface fluxes and brightness temperature are calculated for a diurnal time period (24 h). To analyze the impact of the calibration period, different tests have been performed for the four time intervals (P, P1, P2, and P3) defined in section 2b.

The parameter ranges were fixed following values encountered in the literature, or according to the spatial variability of the measurements performed on the experimental site. For specific parameters or initial conditions an uncertainty of 20% was prescribed. These intervals are specified in Table 2. It is clear that the calibration results depend strongly on the initial ranges of uncertainty of the parameters. In this study the whole range of possible values encountered on the earth's surface has not been taken into account, as was done in Bastidas et al. (1999) and Gupta et al. (1999), because the goal of the paper is to show, in a specific climatic and environmental context, the impact of the dimension of the available calibration dataset on the optimization.

Within the four selected periods, initial parameter ranges were identical except for initialization variables whose initial ranges have been set to the experimental values with a 20% uncertainty. Note that the initial deep soil temperature (T_2) is actually an input variable derived from air temperature with a random error between -2 and $+2$ K, introduced to test the model sensitivity to T_2.

Samples of 6000 simulations were used on each studied period. The size of the simulation set was deduced from different tests performed on the calibration methodology to obtain robust and constant results (increasing the number of simulations and resampling the feasible parameter space). Demarty et al. (2004) showed that a minimum sample size of 1500 simulations was required to eliminate the impact of initial parameter sampling on the sensitivity analysis results of the SiSPAT-RS model.

After the Pareto ranking of the simulations set, the number of selected ranks corresponds to a minimum of 150 simulations. Note that at each iteration, the set of simulations is homogenized and the parameter space is more precisely sampled because of the constant number of simulations (6000). Less than 10 iterations are generally necessary to converge.

a. *Effect of the calibration period on parameter optimization*

The analysis of the different calibration tests shows the impact of the dataset period on the model calibration. As expected, the sensitive parameters are different during the four simulation periods; the importance of the physical processes linked to the soil is larger on the periods P1 and P3. On the contrary, during the second period (P2), the vegetation has a larger impact on the surface fluxes. Such results agree with the conclusions of Demarty et al. (2004) with the SiSPAT-RS model using the same dataset. Their conclusion was that the model was sensitive to the parameters controlling water exchanges near the soil surface as well as in deeper soil layers according to the high evaporative demand of the atmosphere during this period. Consequently, the calibration process does not converge to the same solutions for each period and its evolution along the different iterations may be completely different.

As an example, Fig. 1 presents the result of the calibration tests for the five most sensitive parameters related to the transpiration flux:

$$V_{\max_0},\ l_{\mathrm{gf}},\ dp_2,\ \alpha_{\mathrm{sv}},\quad \text{and}\quad \mathcal{F}_{\mathrm{therm}}.$$

These parameters are key factors for water and energy transfers. Here $V_{\max_0}$ drives the photosynthetic capacity of the canopy and thus the transpiration rate, $\mathcal{F}_{\mathrm{therm}}$ determines soil thermal properties and remains critical in the computation of the soil heat conduction flux, l_{gf} and α_{sv} are vegetation structural and optical properties, and finally, dp_2 is the amount of water available for transpiration (root zone depth); see section c in appendix Ac for more information about the model parameterizations. In the same figure, the variation of the parameter ranges along the iterative process (through the 10 iterations) for these five parameters are plotted for the long-term calibration period P (Fig. 1a) and the three short-term calibration periods (periods P1, P2, and P3 in Fig. 1b). The more sensitive a parameter, the faster the parameter range is reduced along the iterative process.

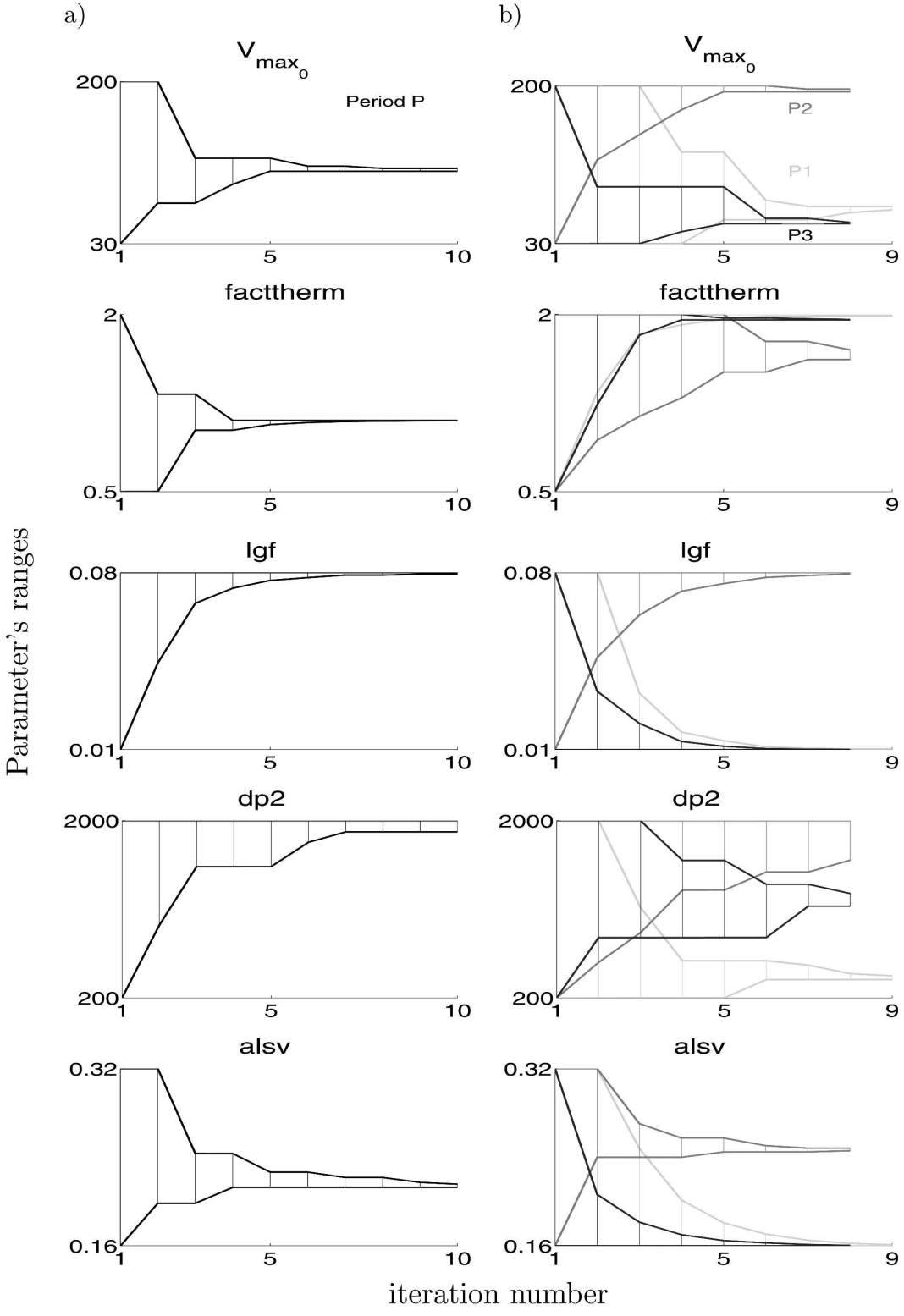

FIG. 1. Parameter range convergence with MCIP for the different periods of calibration (scenario 1): (a) period P; (b) periods P1, P2, and P3.

The main results of the calibration tests are the following: because of the varying surface conditions throughout the year (variation of the LAI and of the vegetation phenology), the surface processes have varying contributions: soil processes are more sensitive during periods P1 with low LAI values and P3 with senescent vegetation and low transpiration. Consequently, parameters like $V_{\max_0}$, l_{gf}, dp_2, and α_{sv} are less sensitive (and on the contrary soil parameters like $\mathcal{F}_{\text{therm}}$ are more sensitive) in period P1 than in the other periods. Moreover, because of the strong precipitation events characterizing period P3, the parameters linked to the hydrodynamic transfers like K_{sat} and n_{VG} are more influential and may be better calibrated. It is worth noting that for all model parameters, and especially these five vegetation parameters, the calibration converges to coherent and realistic values. For example, $V_{\max_0}$ reaches larger values in P2 than in P1 and lower values in P3 in accordance with the expected variations of the transpiration; l_{gf}, dp_2 reach lower values in P3 and P1 than in P2; the same is observed for the vegetation albedo α_{sv}; finally $\mathcal{F}_{\text{therm}}$ calibrated values are larger in P1 and P3 than in P2 where parameter is less sensitive and cannot be calibrated. It is surprising to see that the calibration converges to the same values in period P3 as in P1 while senescent vegetation albedo should be larger than for green vegetation. In fact, it can be explained by the fact that the soil albedo converges to the lower limit of the uncertainty range prescribed; since these values are still too high to match the aR_g measurements, the calibration process tends to decrease the vegetation albedo and reaches the lower limit. These results allow us to show the caveats of the calibration methodology because of the strong dependence of the solution on the initial parameter ranges and on the respective parameter sensitivity to the calibration period. It is to be expected that a long-term calibration will lead to an average solution for the parameter set while a dynamic (short-term) calibration will allow us to better optimize the model simulation for the calibration period. In the latter case, time discontinuities in parameters values will appear from one calibration period to another. It is important to constrain (by a recursive or a preventive way) the parameter ranges to realistic values and to analyze the time correlations between the parameters. One way to limit the errors due to bad calibration (leading to unrealistic parameter estimates) of nonsensitive parameters would be to perform the calibration only on the most sensitive parameters or to guide the optimization process with an a priori solution, which would prevent the nonsensitive parameters from varying much.

b. Comparison of the model performances

The model performance obtained at the end of the calibration process has been compared for the four calibration tests in terms of the rmse and biases on all the variables that have been measured during the Alpilles-ReSeDA experiment, that is, on the six criteria used for the calibration (T_B, w_g, w_2, G, H, and aR_g) as well as criteria on the latent heat flux LE and the net radiation R_n (not used for calibration). The results are summarized in Fig. 2 and Table 3. The statistics are calculated for the experimental dataset (the number of available data for each variable is noted in Table 3 column "N data").

Figure 2 presents the comparison of the rmse obtained during the three simulation periods, P1, P2, and P3, using the calibration set of parameters obtained from the long-term calibration period P, to the simulations obtained with the parameters optimized for the specific short-term periods (dynamic calibration). The results show the following.

- The model performs well in all cases; the rmse values obtained from the whole period as well as from the short-term periods are rather good: the surface fluxes, surface soil moistures, and brightness temperatures are well simulated with rmse values lower than 50 W m^{-2} for the surface fluxes.
- The model performances are generally better with the dynamic calibration except for some variables like the brightness temperature, which can be better simulated with the mean calibration sets. This can be explained easily by referring to the calibration results described above.
- During period P2, since the soil parameters are less sensitive, the calibration is mostly driven by the vegetation parameters, and the soil parameters can be estimated with less accuracy than in the long-term calibration test.
- During periods P1 and P3, on the contrary, the soil parameters determining the hydrologic and thermal transfers are better assessed and, consequently, the soil water content and ground heat flux are better simulated compared to the long-term calibration results.

Nevertheless, the results are quite satisfactory when compared to other SVAT model performances using the same dataset. As a matter of fact, an intercomparison of different SVAT models has been performed in the framework of the Alpilles-ReSeDA program. The results summarized in Olioso et al. (2002b) have been compared to ours. Table 3 gives the bias and rmse for the Alpilles experiment scenario 2 and for the SEtHyS simulation in the same conditions as Olioso et al.

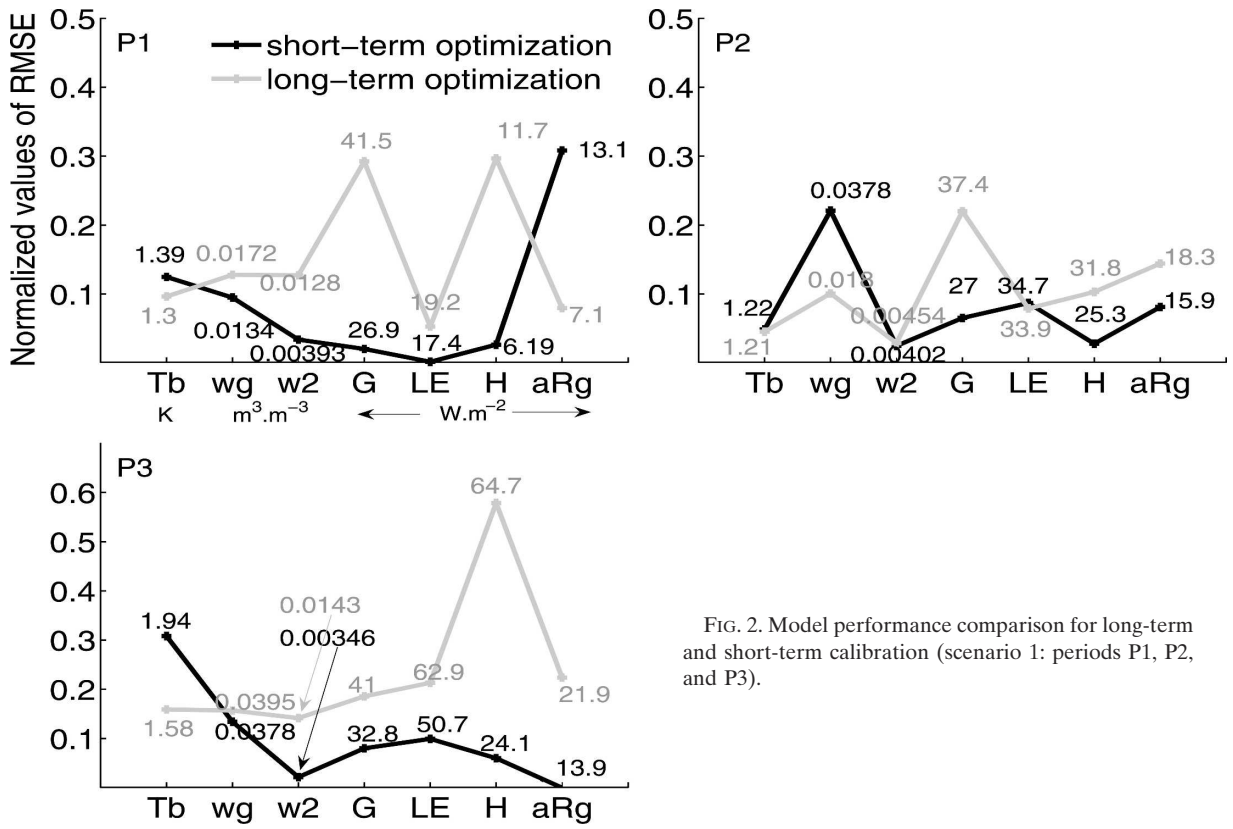

FIG. 2. Model performance comparison for long-term and short-term calibration (scenario 1: periods P1, P2, and P3).

(2002b) intercomparison program (i.e., model runs without calibration). They are compared to the long-term optimization (scenarios 1 and 3). Generally, the model performance is much better in our case when comparing with simple monolayer models, like ISBA (Noilhan and Planton 1989) or Modèle Agrométéorologique d'Evaporation et de Température (MAGRET; Lagouarde 1991), and about the same when comparing with complex multilayer models, like SiSPAT (Braud et al. 1995). Keeping in mind the expected measurement errors, which are around 30 W m^{-2} for the surface fluxes (Olioso et al. 2002a), the SetHyS model results turn out to be quite satisfactory. Results for calibration scenarios 1 and 3 are shown as a comparison. The performance is improved (expected result) for the most complete calibration (scenario 1); scenario 3 is discussed in the next section.

Last, the time series in Fig. 3 show the model performances (DOE 405–415) after the period P1 (DOE 387–407). Surface fluxes LE and *H* are not shown because any measurement time series were available, and soil water contents are plotted from the beginning of period P1 to DOE 415 because of the few measurements and the low variation. Two simulations are plotted: the former is obtained with the short-term calibration for period P1 (plotted here in predictive mode from DOE

TABLE 3. Model performance for the Alpilles experiment long-term calibration: scenarios 1 and 3, DOE 387–542.

	Scenario (long-term optimization: period P)						
	Scenario 1		Alpilles (scenario 2 without calibration)		Scenario 3		
Criterion (rmse)	Bias	Rmse	Bias	Rmse	Bias	Rmse	*N* data
T_B (K)	6.8×10^{-2}	1.38	0.20	1.83	5.6×10^{-2}	1.23	10 903
w_2 (m^3 m^{-3})	-9.3×10^{-3}	1.09×10^{-2}	1.78×10^{-2}	2.18×10^{-2}	1.48×10^{-2}	2.06×10^{-2}	9582
G (W m^{-2})	−2.4	36.8	12.2	45.5	8.9	52.3	11 055
LE (W m^{-2})	3.6	38.7	−12.4	46.7	−15.7	64.4	3358
H (W m^{-2})	−3.7	34.9	−6.1	36.7	2.5	37.7	3358
R_n (W m^{-2})	−6.6	33.9	−5.7	33.6	−10.4	33.4	11 118
aR_g (Wm^{-2})	−2.8	18.6	−1.6	17.2	3.2	20.9	5687

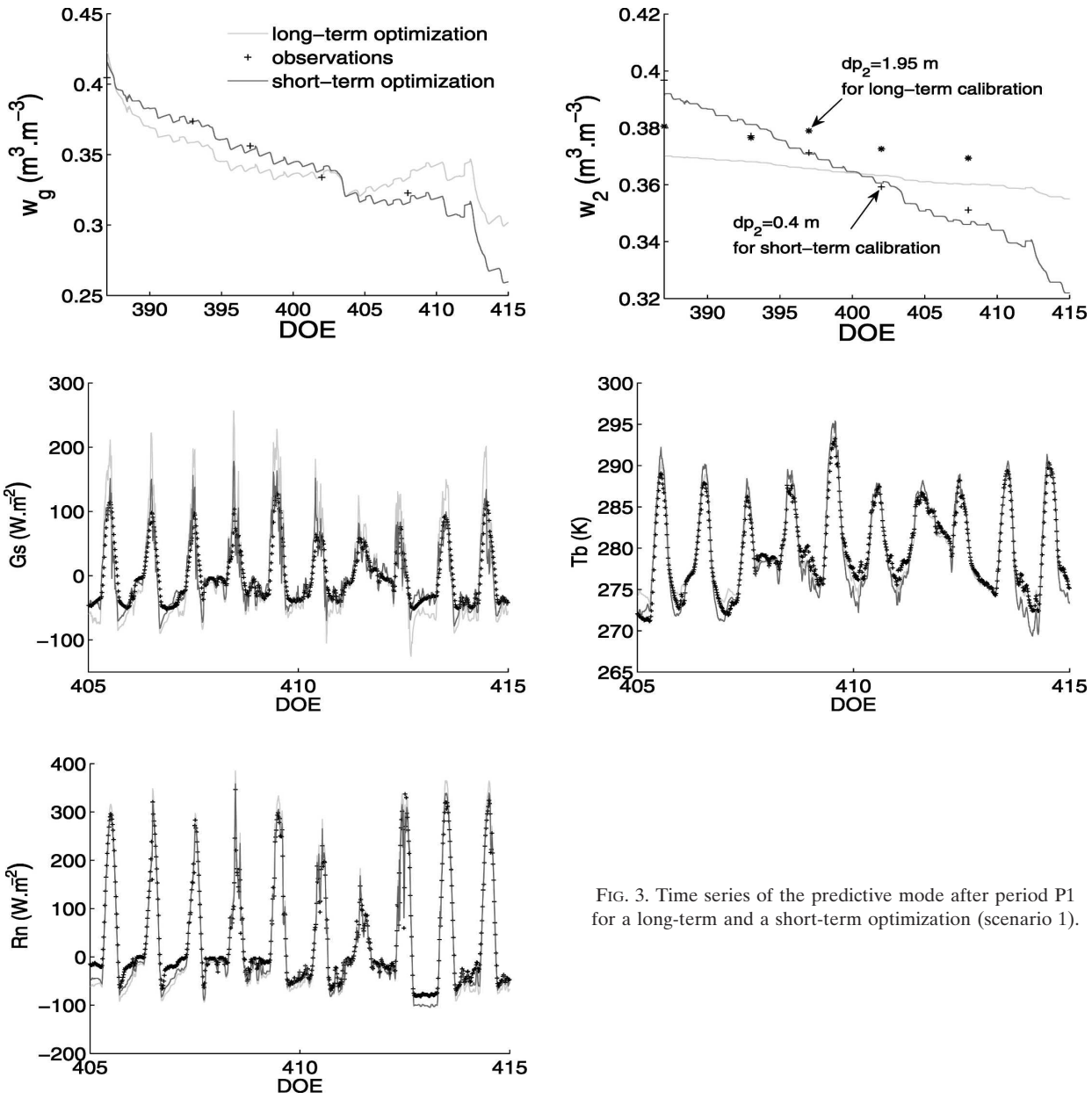

FIG. 3. Time series of the predictive mode after period P1 for a long-term and a short-term optimization (scenario 1).

407 to 415) and the latter corresponds to the parameter set calibrated with long-term optimization for period P. Simulations from short-term optimization better match the observations than the simulations from the average calibration for the 8 days (DOE 407–415) following the short-term calibration period P1. However, the farther the prediction is from the short-term calibation, the more quickly the error increases and the better the simulations from the average calibration perform.

The next section presents results obtained applying the same methodology but reducing the number of calibration variables (without or with only T_B). To understand what necessary information is required to calibrate the SEtHyS model and, more particularly, how the thermal infrared brightness surface temperature may be used to control the model, two additional scenarios have been defined.

5. Contribution of TIR data in model calibration

Additional numerical experiments have been defined to achieve the model calibration with a variable number of criteria. Scenario 2 is the same as the previous scenario 1, but without criterion T_B. This scenario is com-

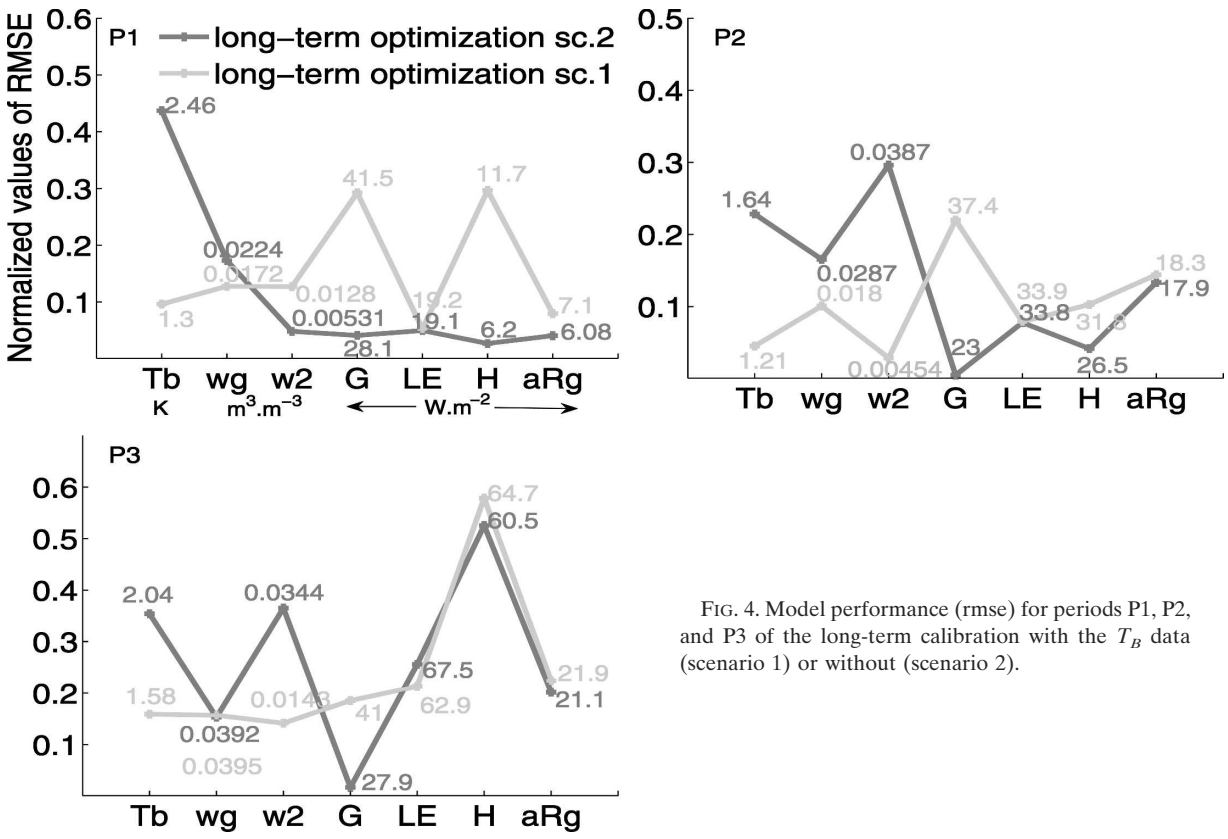

FIG. 4. Model performance (rmse) for periods P1, P2, and P3 of the long-term calibration with the T_B data (scenario 1) or without (scenario 2).

pared to the first one in order to evaluate the contribution of the TIR brightness temperature in multiobjective calibration. Finally, in scenario 3, only the thermal infrared brightness temperature T_B is kept for model calibration (monocriterion study). The main focus of the presentation in this section is on scenarios 2 and 3. Over all the calibration studies, less than 10 iterations of the MCIP methodology were necessary to reach the termination criteria.

At first, it is interesting to qualify and to quantify the contribution of T_B by a comparison of scenarios 1 and 2 where the most documented observation dataset for calibration is used. We have realized a long-term optimization between DOE 387 and 542 (whole crop cycle). The set of reduced parameter ranges obtained afterward has been used for simulating the three periods of interest: P1, P2, and P3. Normalized values of rmse are plotted in Fig. 4; the initial range [0, 1] corresponds to the first iteration of the calibration methodology. Addition of rmse (T_B) (six criteria) permits improvement of the soil water content simulation, and obviously T_B, without compromising the evapotranspiration simulation (or negligible improvement for periods P1 and P3). Figure 4 clearly shows improvement in the minimization of this criteria: for period P2, for example, 1.64 to 1.21 K (26% reduction) for T_B, 2.87×10^{-2} to 1.80×10^{-2} m^3 m^{-3} (37% reduction) for w_g and 3.87×10^{-2} to $0.45.10^{-2}$ m^3 m^{-3} (88% reduction) for w_2. Note that errors in simulation of ground heat flux G (23 to 37.4 W m^2, + 63%) and sensible heat flux H (26.5 to 31.8 W m^{-2}, + 20%) increase. For the three different periods, the improvement in soil water content and brightness temperature simulation (evapotranspiration is also improved for period P3) due to the contribution T_B is associated with the increase of G and H flux simulation errors.

For the SEtHyS SVAT model, the T_B data has at least a real impact on error compensation between the mass and energy budget physical processes. Scenarios 1 and 2 show which influential parameters are responsible for the discrepancies in criteria minimization. Considering both long-term and short-term optimization cases, the 9 following sensitive parameters (over the 22 model parameters)—ε_g, $\mathcal{F}_{\text{therm}}$, $V_{\max_0}$, $w_{\max}$, K_{sat}, n_{VG}, $a_{E\text{lim}}$, $b_{E\text{lim}}$, and dp_2—converge on quite different values of the initial ranges for the scenarios 1 and 2. These parameters are the most directly influential ones in the calculation of the brightness temperature. Some of these parameters are less constrained without the T_B criteria, and the optimization converges toward differ-

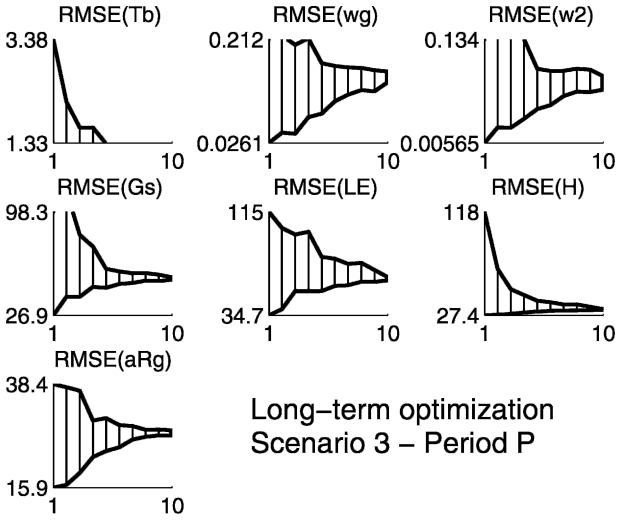

FIG. 5. Model performance for period P of a long-term calibration with only T_B (scenario 3); ranges of rmse for the different variables are plotted for each iteration of the iterative calibration process.

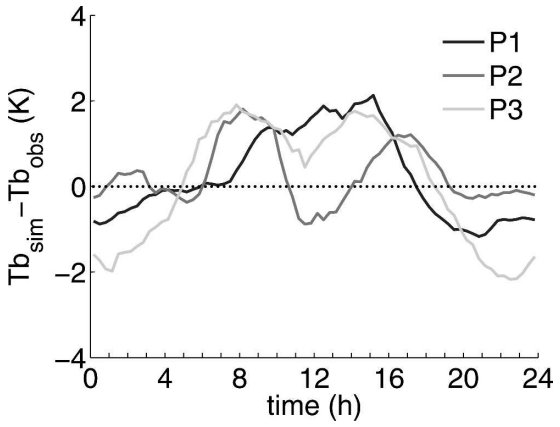

FIG. 6. Mean difference of brightness temperature (T_B simulation minus T_B observation) after a short-term calibration for periods P1, P2, and P3: scenario 1. The average day is plotted for each period.

ent solutions. This is the case for the bare ground emissivity ε_g, which takes a lower value of the initial range (0.94) and leads to a larger error for the surface temperature simulation. Parameter $\mathcal{T}_{\text{therm}}$ is less constrained and converges on extreme values of the initial range criteria, unlike in scenario 1; $V_{\max_0}$, $a_{E\text{lim}}$, $b_{E\text{lim}}$, and dp_2 are sensitive in T_B determination in an indirect way because they regulate the evapotranspiration rate. As for $w_{\max}$, K_{sat}, and n_{VG}, these parameters are relevant in determining the hydrologic transfer calculation and consequently the soil moisture simulation, which affects thermal soil conditions and evapotranspiration. It can be noted that the parameter n_{VG} is the most influential parameter of the retention curve in dry conditions (periods P2 and P3).

Surface brightness temperature data plays an important role in model calibration as shown previously. Moreover, long-term optimization using criteria T_B permits improvements of the soil moisture simulation (and potentially evapotranspiration flux). However, it is necessary to determine the impact on model calibration at field scale when only T_B is used in the optimization methodology.

Thus, the last scenario (scenario 3) consists of minimization of the only rmse(T_B). The calibration methodology applied for period P (DOE 387–542, long-term optimization) gives the results presented Fig. 5.

The reduction of the criteria ranges, iteration after iteration, clearly illustrates the quick minimization of rmse(T_B). The other criteria are not, in general, minimized [except rmse(H)]. Particularly, criteria on soil water content tend to values greater than the medium of initial ranges. An important consequence is that the monitoring of soil moisture with brightness temperature needs to be improved and cannot be managed in this way. As a matter of fact, initial soil water contents tend to extreme values of their respective initial ranges after the calibration methodology. Parameters linked to evapotranspiration converge on values that limit the latent heat flux, $V_{\max_0}$ (constraining photosynthetic assimilation rate), tends to lower values of the initial range, about 40 μmol m^{-2} s^{-1}. Emissivity ε_g tends to the maximal one (0.99) and $\mathcal{T}_{\text{therm}}$ to values less than 1 (increasing heat soil capacity). The consequence on simulation is an overestimated G flux amplitude and an underestimated LE during the day. The optimization of rmse(T_B) tends globally to reduce the diurnal cycle amplitude and limit evapotranspiration flux (compared to the multiobjective calibration), which is a priori paradoxical (see below). Short-term optimizations for periods P1, P2, and P3 are influenced by the characteristics of the discrepancies between simulations and observations (model errors).

Figure 6 illustrates the mean differences of T_B (between simulation and observation) after the six-criteria short-term calibration (scenario 1) over the three periods. A total positive bias (0.23 K for period P1, 0.27 K for period P2, and 0.1 K for period P3) of the simulations is observed: calibration with a larger relative weight on criterion T_B will lead to a preferential calibration of the processes directly linked to the surface temperatures (soil and vegetation) and will converge to very different solutions compared to the six-criteria case (scenario 1). Average features allow the understanding of the monocriterion calibration results based on the minimization of rmse(T_B) (scenario 3). Actually, the curves for the three periods underline a negative

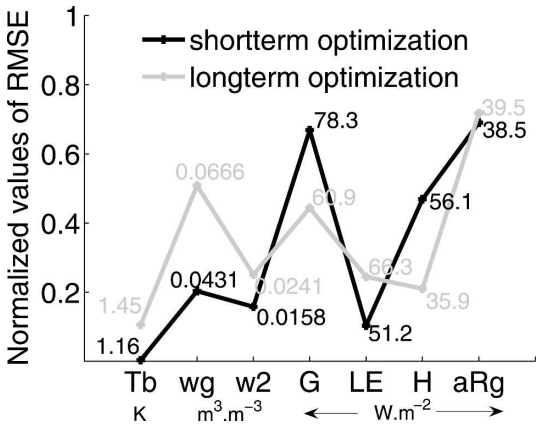

FIG. 7. Model performance for period P3 long-term and short-term calibration: scenario 3 (T_B data are only used for calibration).

(positive) bias during the night (daytime). Curves relative to periods P2 and P3 exhibit a similar shape (with different time shifting and amplitude offset). For these two periods canopy is more developed (greater LAI) than for period P1, and the observed feature near midday is relevant to canopy transpiration. Short-term calibration for period P1 tends to minimize the positive bias during the day, and the parameterization favors soil evaporation ($a_{E\mathrm{lim}}$ and $b_{E\mathrm{lim}}$ take the higher values of the initial ranges, about 50). During period P1, the contribution of vegetation is very low (LAI is lower than 0.56) and the soil evaporation provides a larger contribution to the total latent heat flux. For period P2, canopy transpiration must be reduced near midday to increase the surface temperature. This is relevant to the fact that transpiration is the main physical process to control temperature at this time of day. Parameters take values in order to globally reduce the surface temperature in daytime and increase it near midday. Soil heat capacity is increased via lower values of the $\mathcal{F}_{\mathrm{therm}}$ parameter. In fact, the calibrated values decreased from 1.65 in the six-criteria study (scenario 1) to 0.71 in the monocriterion study (scenario 3). The same features are observed for period P3. The consequence on the surface flux errors at the end of the calibration is an underestimation of the simulated latent heat flux and an overestimation of the ground heat flux.

However, short-term calibration for the three periods leads to an important result: the minimization of rmse(T_B) is correlated with the minimization of G and LE fluxes for period P1, of w_2 and H for period P2, and of w_2, w_g, and LE for period P3 as shown by Fig. 7. Thus, total soil water content w_2 could be controlled by the brightness temperature T_B when the canopy is developed enough (periods P2 and P3). Note that initial soil water content w_{2_0} is retrieved compared to the observations.

Figure 7 indicates a short-term optimization (20 days here) compared to a long-term one over the whole crop cycle (155 days in our case) leading to a mean calibrated parameter set. Actually, short-term calibration allows improvement of criterion LE for all periods and, also for example, T_B, w_g, and w_2, for period P3. Short-term calibration with criterion T_B leads to minimization of other criteria compared to long-term optimization. However, this improvement is compensated for the larger error on the remaining criteria. This result is not directly usable but means that the dynamics of T_B contains a powerful information to preferentially calibrate some model parameters over short periods and thus improve the model performance.

Finally, these numerical experiments permit one to better understand the role of TIR data in model calibration and to underline the necessity of taking advantage of the dynamics of T_B on short-term periods to constrain the dominant processes of the energy and water balance.

6. Summary and conclusions

The different numerical experiments performed in this study were inspired by the previous work of Bastidas et al. (1999), Gupta et al. (1999), and Demarty et al. (2004, 2005). In our case the methodology was applied to the SEtHyS model, and the objective was to analyze the potentialities of TIR remote sensing measurements for SVAT model calibration. Three scenarios have been defined to understand the model optimization behavior according to the climatic and environmental conditions. Multicriteria model calibrations (scenarios 1 and 2) were achieved over four simulation periods. We have shown that the influential parameters and their preferential values are quite different along the period of simulation (depending on the respective contributions of soil and vegetation) and that the feasible parameter space consequently varies with time. This result underlines the possibility of improving the calibration by implementing a dynamic calibration strategy (short-term optimization). In fact, the active and growing vegetation period P2 shows a larger sensitivity of the parameters related to the evapotranspiration processes. Meanwhile the period P1 concerns sensitive parameters linked to radiative properties and soil heat flux. Moreover, the parameter sensitivity varies throughout the day with the physical processes involved. For example, the parameters governing the transpiration process will show a larger sensitivity around midday, whereas the parameters involved in soil heat fluxes will be more influential the rest of the day. Thus, it is clear that the choice of calibration pe-

riods both diurnally and during the vegetation cycle should permit optimization of the calibration process.

Comparison between scenarios 1 and 2 clearly illustrates the contribution of T_B to the multiobjective calibration process. Minimization of criteria T_B allows improvement of soil water content and evapotranspiration criteria with long-term calibration. However, the errors in the brightness temperature, and especially the biases that have been noted on the short-term calibration periods, prevent the calibration process from succeeding when only T_B is used for calibration. As already noted by different authors (Gupta et al. 1999; Margulis and Entekhabi 2003), it is very important to analyze the causes of these discrepancies before performing a model calibration. The monitoring of these biases is still an open question. Indeed, in our case, the temperature bias varies with time throughout the simulation and is quasi-null when averaged over all the studied periods. This result strengthens the necessity of analyzing the impacts of the choice of calibration periods and adjusting them optimally. When T_B is the only criterion used for calibration (scenario 3), the results are not as good as in the first two scenarios. However, the use of only T_B for short-term calibration appears to be promising because the minimization of T_B criterion allows the improvement of other criteria. The challenge consists now of developing a calibration methodology that will take advantage of not only the time-varying model parameter influence but also the time availability of the observations and the dynamics of the T_B diurnal cycle to improve the model calibration methodology without biasing the results.

Acknowledgments. This work was funded by the French national programs: Programme National de Télédétection Spatiale (PNTS) and Programme National de Recherches en Hydrologie (PNRH), with support of Centre National d'Etudes Spatiales (CNES), Office National d'Etudes et de Recherches Aérospatiales (ONERA), and Réseau Terre Espace (RTE) program, from which B. Coudert, P. Guillevic, and B. Boudevillain received Ph.D. and postdoctoral grants. The Alpilles-ReSeDA program was funded by the EEC-DG XII (Contract ENV4-CT96-0326-PL-952071).

The authors wish to acknowledge Albert Olioso and anonymous reviewers for their constructive suggestions. Additions and corrections suggested by Steven Margulis were very helpful.

APPENDIX

The SEtHyS SVAT Model

This section presents a description of the soil–vegetation–atmosphere continuum parameterization.

a. Radiative budget

Vegetation density is a determining factor in partitioning the downward solar radiative flux. The radiation partition is a function of a shielding factor σ_f (Deardorff 1978) depending on the leaf area index. The following expressions of the σ_f factor are used in both shortwave and longwave domains, assuming a spherical distribution of leaves (François 2002):

$$\begin{cases} \sigma_f = 1 - e^{(-0.825\mathrm{LAI})} & \text{for longwave domain} \\ \sigma_f = 1 - e^{(-0.5\mathrm{LAI})} & \text{for shortwave domain} \end{cases}. \tag{A1}$$

The radiation balance is then solved simultaneously at ground and canopy levels for shortwave and longwave radiation. In the shortwave domain, soil albedo α_{sg} is assumed to be linearly dependent on surface soil moisture (see parameters list). Foliage albedo α_{sf} is a parameter of the model.

Thus, the expression of the shortwave net radiation is at ground level:

$$R_{\mathrm{sg}} = S^{\downarrow} \frac{(1 - \sigma_f)(1 - \alpha_{\mathrm{sg}})}{1 - \sigma_f \alpha_{\mathrm{sg}} \alpha_{\mathrm{sf}}} \tag{A2}$$

and at canopy level:

$$R_{\mathrm{sf}} = S^{\downarrow}(1 - \alpha_{\mathrm{sf}})\sigma_f \left[1 + \alpha_{\mathrm{sg}} \frac{(1 - \sigma_f)}{1 - \sigma_f \alpha_{\mathrm{sg}} \alpha_{\mathrm{sf}}} \right], \tag{A3}$$

where $S^{\downarrow}$ is the incoming shortwave radiation.

In the longwave domain, assuming that canopy and ground emissivity are known (ε_f and ε_g are input parameters), longwave net radiation is given at ground level by

$$R_{\mathrm{Lg}} = (1 - \sigma_f) \frac{\varepsilon_g (R^{\downarrow} - \sigma T_g^4)}{1 - \sigma_f (1 - \varepsilon_f)(1 - \varepsilon_g)} - \frac{\varepsilon_g \varepsilon_f \sigma_f \sigma (T_g^4 - T_f^4)}{1 - \sigma_f (1 - \varepsilon_f)(1 - \varepsilon_g)} \tag{A4}$$

and at canopy level by

$$R_{\mathrm{Lf}} = \sigma_f \left[\varepsilon_f (R^{\downarrow} - \sigma T_f^4) + \frac{\varepsilon_g \varepsilon_f \sigma (T_g^4 - T_f^4)}{1 - \sigma_f (1 - \varepsilon_f)(1 - \varepsilon_g)} \right] + \sigma_f \frac{(1 - \varepsilon_f)(1 - \varepsilon_g)\varepsilon_f (R^{\downarrow} - \sigma T_f^4)}{1 - \sigma_f (1 - \varepsilon_f)(1 - \varepsilon_g)}. \tag{A5}$$

Direct solar shortwave radiation $S^{\downarrow}$ and atmospheric longwave radiation $R^{\downarrow}$ are input model data.

The thermal infrared surface temperature T_B (observed above the canopy) results from the partitioning of the surface and the radiative interaction between soil (whose temperature is T_g) and the vegetation above (whose temperature is T_f).

b. Heat fluxes expressions

The mass and energy transfers in equilibrium with net surface radiation are momentum, sensible, and latent heat fluxes. A conductance formalism allows expressing them by considering the canopy as a single vegetation layer (at some height Z_{af}) above ground (Thom 1972). Thus, following the electrical (Ohm's law) analogy, soil surface, leaf surface, air canopy space, and atmosphere above canopy are the levels between which differences of potential (temperature and humidity gradients) and transfer coefficients, that is, aerodynamic conductances, can be calculated.

Heat fluxes H and LE (sensible and latent heat fluxes, respectively) are then determined at three levels,

1) atmospheric reference level:

$$H = \rho c_p C_h (T_{av} - T_a) \tag{A6}$$

$$\mathrm{LE} = \frac{\rho c_p}{\gamma} C_h (q_{av} - q_a) \tag{A7}$$

2) vegetation level:

$$H_v = \rho c_p C_{hv} (T_v - T_{av}) \tag{A8}$$

$$\mathrm{LE}_v = \frac{\rho c_p}{\gamma} C_{hv} R' [q_{sat}(T_v) - q_{av}] \tag{A9}$$

3) ground level:

$$H_g = \rho c_p C_{hg} (T_g - T_{av}) \tag{A10}$$

$$\mathrm{LE}_g = \frac{\rho c_p}{\gamma} C_{hg} C_s [q_{sat}(T_g) - q_{av}] \tag{A11}$$

with

$$\mathrm{LE} = \mathrm{LE}_g + \mathrm{LE}_v \tag{A12}$$

$$H = H_g + H_v, \tag{A13}$$

where c_p is the specific heat at constant pressure; γ is the psychrometric constant; T and q are temperature and water vapor pressure; and a, v, av, and g are indices relative to air, vegetation, canopy air space, and ground.

Respectively, C_h, C_{hv}, and C_{hg} are aerodynamic conductances between canopy air space and the overlaying atmosphere, leaf surface and canopy air space, and ground and canopy air space; the R' factor is defined below. These variables are derived from the eddy flux theory between two atmospheric levels. In the SEtHyS model, the formulation follows the parameterization proposed by Shuttleworth and Wallace (1985). A constant extinction coefficient in the exponential wind speed profile value for crops (2.5) is considered between atmospheric and canopy air space levels.

Here C_s is the ground evaporation conductance; it depends on soil moisture conditions and potential evaporation E_{gpot} (Bernard et al. 1986; Wetzel and Chang 1988; Soarès et al. 1988):

$$C_s = \min\left(1, \frac{E_{lim}}{E_{gpot}}\right), \tag{A14}$$

where E_{lim} depends on soil properties (composition and moisture). Soarès et al. (1988) gives the expression

$$E_{lim} = a_{Elim}\{\exp[b_{Elim}(w_g - w_{resid})^2] - 1\}, \tag{A15}$$

where a_{Elim} and b_{Elim} are model parameters related to soil evaporation response.

In Eq. (A9) the R' factor accounts for stomatal resistance and that only the fraction of the canopy area not covered by water will contribute to evapotranspiration. Deardorff (1978) proposed the expression

$$R' = \left(\frac{\mathrm{dew}}{d_{max}}\right)^{2/3} + \left[1 - \left(\frac{\mathrm{dew}}{d_{max}}\right)^{2/3}\right] \frac{1}{(\beta + C_{fh}\mathrm{RST})}, \tag{A16}$$

$R' = 1$ for condensation,

where "dew" ("d_{max}") is the fraction (the maximal one) of free water on the foliage. RST is the stomatal resistance; this factor governs the canopy participation to the energy budget and is responsible for partition between sensible and latent heat fluxes.

In the model, calculation of RST is based on Collatz et al. (1991, 1992) and is the same as in SiB models (Sellers et al. 1992, 1996). Biophysical and environmental variables manage photosynthesis processes giving CO_2 assimilation rate and then stomatal conductance of the foliage.

Ball (1988) gives the following leaf stomatal conductance expression:

$$g_s = m \frac{A_n}{c_s} h_s p + b, \tag{A17}$$

where A_n is net assimilation rate calculated by the model of Farquhar et al. (1980), c_s and h_s are CO_2 partial pressure and relative humidity at leaf surface, p is atmospheric pressure, and m and b are empirical fac-

tors from observations depending on vegetation type (C_3 or C_4).

Assimilation rate is determined by means of three factors: a photosynthetic enzyme (Rubisco) limiting rate, a light limiting rate, and a limiting rate owing to the leaf capacity to export or utilize the photosynthesis products (Collatz et al. 1991). In the model, the iterative solution method for the photosynthesis–stomatal conductance calculation proposed by Collatz et al. (1991) has been implemented. Indeed, canopy is considered as a "big leaf," assuming bulk or integral values over canopy depth used in the integrated form of Eq. (A17) (see Sellers et al. 1992). Stomatal conductance and net assimilation rate are then determined for the canopy.

c. Governing equations for SEtHyS prognostic variables

The soil surface temperature T_g, the vegetation temperature T_v, the air temperature inside the canopy T_{av}, and the air humidity inside the canopy q_{av} are determined by a first-order linearization of the following mass and energy budget system:

$$\begin{cases} R_{n_g} = H_g + \mathrm{LE}_g + G \\ R_{n_v} = H_v + \mathrm{LE}_v \\ H = H_v + H_g \\ E = E_v + E_g, \end{cases} \tag{A18}$$

where R_{ng} and R_{nv} are net radiations at ground and canopy levels and G is the ground heat flux. Parameterization of the soil behavior is based on Deardorff's (1978) formalism. Soil surface temperature method prediction is, namely, the force–restore method (Bhumralkar 1975; Blackadar 1976) and requires deep soil temperature T_2; T_2 can be estimated from the mean air temperature over the previous 24 hours for short-range studies (Blackadar 1976). A good approximation of T_2 may be obtained in our case of study (larger range) by averaging the air temperature above the surface over a 2-week period preceding the day of simulation on the Alpilles-ReSeDA site (Coudert 2003). The heat capacity is prescribed by the de Vries (1963) model , and hydrodynamic properties result from pedotransfer functions (retention curve, hydraulic conductivity) based on the Van Genuchten (1980) approach under the Mualem (1976) hypothesis. The prognostic equation for ground surface temperature is written as

$$\frac{\partial T_g}{\partial t} = \frac{2\sqrt{\pi}}{C_e}(R_n - H - \mathrm{LE}) - \frac{2\pi}{\tau}(T_g - T_2). \tag{A19}$$

The factor C_e is an equivalent heat capacity related to the diurnal thermal wave damping layer. In our model, the parameterization of the equivalent heat capacity has been weighted by introducing an empirical factor ("F_{therm}" in parameters list; Table 2) compared to Deardorff (1978).

Deardorff (1978) proposed a similar treatment of ground soil moisture, leading to the following equations:

$$\frac{\partial w_g}{\partial t} = -\left[E_g + 0.2E_v\left(\frac{w_g}{w_{\max}}\right) - P\right]/dp_1 - C(w_g, w_2)(w_g - w_2), \tag{A20}$$

$$\frac{\partial w_2}{\partial t} = -\frac{E_g + E_v - P}{dp_2}, \tag{A21}$$

where $w_{\max}$ is the soil moisture at soil saturation, w_g and w_2 are surface and root zone water contents, P is the precipitation rate, and dp_1 and dp_2 are the surface and root zone layers depths.

REFERENCES

Ball, J. T., 1988: An analysis of stomatal conductance. Ph.D. thesis, Stanford University, 89 pp.

Bastidas, L. A., H. Gupta, S. Sorooshian, W. Shuttleworth, and Z. Yang, 1999: Sensitivity analysis of a land surface scheme using multicriteria methods. *J. Geophys. Res.,* **104,** 19 481–19 490.

Bernard, R., J. V. Soares, and D. Vidal-Madjar, 1986: Differential bare field drainage properties from airborne microwave observations. *Water Resour. Res.,* **22,** 869–875.

Bhumralkar, C., 1975: Numerical experiments on the computation of ground surface temperature in an atmospheric general circulation model. *J. Appl. Meteor.,* **14,** 1246–1258.

Blackadar, A., 1976: Modeling the nocturnal boundary layer. Preprints, *Third Symp. on Atmospheric Turbulence Diffusion with Second Air Quality,* Raleigh, NC, Amer. Meteor. Soc., 46–49.

Braud, I., A. Dantas-Antonio, and M. Vauclin, 1995: A stochastic approach to studying the influence of the spatial variability of soil hydraulic properties on surface fluxes, temperature and humidity. *J. Hydrol.,* **165,** 283–310.

Collatz, G., J. Ball, C. Grivet, and J. Berry, 1991: Physiological and environmental regulation of stomatal conductance, photosynthesis and transpiration: A model that includes a laminar boundary layer. *Agric. For. Meteor.,* **54,** 107–136.

——, M. Ribas-Carbo, and J. Berry, 1992: Coupled photosynthesis-stomatal conductance model for leaves of C_4 plants. *Aust. J. Plant Physiol.,* **19,** 519–538.

Coudert, B., 2003: Etude de sensibilité du modèle d'interface SEtHyS: Application au suivi de l'état hydrique des sols par assimilation de données. CETP-IPSL Internal Rep., 30 pp.

Deardorff, J. W., 1978: Efficient prediction of ground surface temperature and moisture, with inclusion of a layer of vegetation. *J. Geophys. Res.,* **83,** 1889–1903.

Demarty, J., C. Ottlé, I. Braud, A. Olioso, J. P. Frangi, L. A. Bastidas, and H. V. Gupta, 2004: Using a multiobjective ap-

proach to retrieve information on surface properties used in a SVAT model. *J. Hydrol.,* **287,** 214–236.

——, ——, ——, ——, ——, H. V. Gupta, and L. A. Bastidas, 2005: Constraining a physically based Soil–Vegetation–Atmosphere Transfer model with surface water content and thermal infrared brightness temperature measurements using a multiobjective approach. *Water Resour. Res.,* **41,** W01011, doi:10.1029/2004WR003695.

de Vries, D., 1963: Thermal properties of soils. *Physics of Plant Environment,* V. Wijik, Ed., North-Holland, 210–235.

Diak, G., J. Mecikalski, M. Anderson, J. Norman, W. Kustas, R. Torn, and R. DeWolf, 2004: Estimating land surface budgets from space. *Bull. Amer. Meteor. Soc.,* **85,** 65–78.

Dickinson, R. E., A. Henderson-Sellers, and P. J. Kennedy, 1993: Biosphere–Atmosphere Transfer Scheme (BATS) version le as coupled to the NCAR Community Climate Model. NCAR Tech. Note NCAR/TN-387+STR, 72 pp.

Duan, Q., V. Gupta, and S. Sorooshian, 1993: A shuffled complex evolution approach for effective and efficient global minimization. *J. Optim. Theory Appl.,* **76,** 501–521.

Farquhar, G., S. von Caemmerer, and J. Berry, 1980: A biochemical model of photosynthetic CO_2 assimilation in leaves of C_3 species. *Planta,* **149,** 78–90.

François, C., 2002: The potential of directional radiometric temperatures for monitoring soil and leaf temperature and soil moisture status. *Remote Sens. Environ.,* **80,** 122–133.

——, C. Ottlé, and L. Prévot, 1997: Analytical parameterization of canopy directional emissivity and canopy directional radiance in the thermal infrared, application on the retrieval of soil and foliage temperatures using two directional measurements. Part 1: Theory. *Int. J. Remote Sens.,* **18,** 2587–2621.

Gupta, H. V., L. Bastidas, S. Sorooshian, W. Shuttleworth, and Z. L. Yang, 1999: Parameter estimation of a land surface scheme using multicriteria methods. *J. Geophys. Res.,* **104,** 19 491–19 503.

Hornberger, G. M., and R. Spear, 1981: An approach to the preliminary analysis of environmental systems. *J. Environ. Manage.,* **12,** 7–18.

Jia, L., Z. L. Li, M. Menenti, Z. B. Su, W. Verhoef, and Z. Wan, 2003: A practical algorithm to infer soil and foliage component temperatures from bi-angular ATSR-2 data. *Int. J. Remote Sens.,* **24,** 4739–4760.

Lagouarde, J. P., 1991: Use of NOAA AVHRR data combined with an agrometeorological model for evaporation mapping. *Int. J. Remote Sens.,* **12,** 1853–1864.

Margulis, S. A., and D. Entekhabi, 2003: Variational assimilation of radiometric surface temperature and reference-level micrometeorology into a model of the atmospheric boundary layer and land surface. *Mon. Wea. Rev.,* **131,** 1272–1288.

Menenti, M., L. Jia, Z. L. Li, V. Djepa, J. Wang, M. P. Stoll, Z. B. Su, and M. Rast, 2001: Estimation of soil and vegetation temperatures with directional thermal infrared observations: The IMGRASS, HEIFE and SGP'97 experiments. *J. Geophys. Res.,* **106,** 11 997–12 010.

Mualem, Y., 1976: A new model for predicting the hydraulic conductivity of unsaturated porous media. *Water Resour. Res.,* **12,** 513–521.

Noilhan, J., and S. Planton, 1989: A simple parameterization of land surface processes for meteorological models. *Mon. Wea. Rev.,* **117,** 536–549.

Norman, J., W. Kustas, and K. Humes, 1995: A two source approach for estimating soil and vegetation energy fluxes from observations of directional radiometric surface temperature. *Agric. For. Meteor.,* **77,** 153–166.

Olioso, A., and Coauthors, 2002a: Monitoring energy and mass transfers during the Alpilles-ReSeDA experiment. *Agronomie,* **22,** 597–610.

——, and Coauthors, 2002b: SVAT modeling over the Alpilles-ReSeDA experiment: Comparing SVAT models over wheat fields. *Agronomie,* **22,** 651–668.

Sellers, P., J. A. Berry, G. Collate, C. Field, and F. Hall, 1992: Canopy reflectance, photosynthesis, and transpiration. III. A reanalysis using improved leaf models and a new canopy integration scheme. *Remote Sens. Environ.,* **42,** 187–216.

——, and Coauthors, 1996: The ISLSCP Initiative I global datasets: Surface boundary conditions and atmospheric forcings for land–atmosphere studies. *Bull. Amer. Meteor. Soc.,* **77,** 1987–2005.

Shuttleworth, W., and J. S. Wallace, 1985: Evaporation from sparse crops—An energy combination theory. *Quart. J. Roy. Meteor. Soc.,* **111,** 839–855.

Soarès, J., R. Bernard, O. Taconet, D. Vidal-Madjar, and A. Weill, 1988: Estimation of bare soil evaporation from airborne measurements. *J. Hydrol.,* **99,** 281–296.

Spear, R., and G. Hornberger, 1980: Eutrophication of peel inlet. II. Identification of critical uncertainties via generalized sensitivity analysis. *Water Resour. Res.,* **14,** 43–49.

Thom, A., 1972: Momentum, mass and heat exchange of vegetation. *Quart. J. Roy. Meteor. Soc.,* **98,** 124–134.

Van Genuchten, M., 1980: A closed-form equation for predicting the hydraulic conductivity of unsaturated soils. *Soil Sci. Soc. Amer. J.,* **44,** 892–898.

Wetzel, P., and J.-T. Chang, 1988: Evapotranspiration from nonuniform surfaces: A first approach for short-term numerical weather prediction. *Mon. Wea. Rev.,* **116,** 600–621.

Yapo, P. O., H. Gupta, and S. Sorooshian, 1998: Multi-objective global optimization for hydrologic models. *J. Hydrol.,* **204,** 83–97.

Young, P., 1978: A general theory of modeling for badly defined dynamic systems. *Modeling, Identification, and Control in Environmental Systems*, G. Vansteenkiste, Ed., North-Holland, 103–135.